Mixing and transport during pharmaceutical twin-screw wet granulation: experimental analysis via chemical imaging

Ashish Kumar[a,b], Jurgen Vercruysse[c], Maunu Toiviainen[d], Pierre-Emmanuel Panouillot[d], Mikko Juuti[d], Valérie Vanhoorne[c], Chris Vervaet[c], Jean Paul Remon[c], Krist V. Gernaey[d], Thomas De Beer[b,1], Ingmar Nopens[a,*]

[a] *BIOMATH, Dept. of Mathematical Modelling, Statistics and Bioinformatics, Faculty of Bioscience Engineering, Ghent University, Coupure Links 653, B- 9000 Gent, Belgium*
[b] *Laboratory of Pharmaceutical Process Analytical Technology, Dept. of Pharmaceutical Analysis, Faculty of Pharmaceutical Sciences, Ghent University, Harelbekestraat 72, B-9000 Ghent, Belgium*
[c] *Laboratory of Pharmaceutical Technology, Dept. of Pharmaceutics, Faculty of Pharmaceutical Sciences, Ghent University, Harelbekestraat 72, B-9000 Ghent, Belgium*
[d] *Center for Process Engineering and Technology, Department of Chemical and Biochemical Engineering, Technical University of Denmark, DK-2800 Kongens Lyngby, Denmark*

Abstract

Twin-screw granulation is a promising continuous alternative for traditional batch high shear wet granulation (HSWG). The extent of HSWG in a twin screw granulator (TSG) is greatly governed by the residence time of the granulation materials in the TSG and degree of mixing. In order to determine the residence time distribution (RTD) and mixing in TSG, mostly visual observation and particle tracking methods are used, which are either inaccurate and difficult for short RTD, or provide an RTD only for a finite number of preferential tracer paths. In this study, near infrared chemical imaging, which is more accurate and

*Email address: ingmar.nopens@ugent.be, Tel.: +32 (0)9 264 61 96; fax: +32 (0)9 264 62 20
Email addresses: ashish.kumar@ugent.be (Ashish Kumar), jurgen.vercruysse@ugent.be (Jurgen Vercruysse), maunu.toiviainen@vtt.fi (Maunu Toiviainen), pierre-emmanuel.panouillot@vtt.fi (Pierre-Emmanuel Panouillot), mikko.juuti@vtt.fi (Mikko Juuti), valerie.vanhoorne@ugent.be (Valérie Vanhoorne), chris.vervaet@ugent.be (Chris Vervaet), jeanpaul.remon@UGent.be (Jean Paul Remon), kvg@kt.dtu.dk (Krist V. Gernaey), thomas.debeer@ugent.be (Thomas De Beer)
URL: www.biomath.ugent.be (Ingmar Nopens)
[1] Shared last authorship

provides a complete RTD, was used. The impact of changes in material throughput (10-17 kg/h), screw speed (500-900 rpm), number of kneading discs (2-12) and stagger angle (30-90°) on the RTD and axial mixing of the material was characterised. The experimental RTD curves were used to calculate the mean residence time, mean centred variance and the Péclet number to determine the axial mixing and predominance of convective over dispersive transport. The results showed that screw speed is the most influential parameter in terms of RTD and axial mixing in the TSG and established a significant interaction between screw design parameters (number and stagger angle of kneading discs) and the process parameters (material throughput and number of kneading discs). The results of the study will allow the development and validation of a transport model capable of predicting the RTD and macro-mixing in the TSG. These can later be coupled with a population balance model in order to predict granulation yields in a TSG more accurately.
Keywords: twin-screw granulation, residence time distribution, axial mixing, NIR chemical imaging

---

1. Introduction

In the pharmaceutical industry, the main purpose of granulation is to enlarge particles to improve flowability for better downstream processing, while reducing the variability in the formulation mixture. Twin-screw granulation, which is seen as a promising continuous alternative for traditional batch high shear wet granulation (HSWG), allows a relatively high material throughput with a short residence time (typically few seconds) [1]. In a twin-screw granulator (TSG), besides homogeneous distribution of granulation material, the aim is also to achieve mixing within the shortest screw lengths and at minimum required power input. This is important to govern the extent of different rate processes such as wetting, growth and breakage, which ultimately determine the characteristics of the produced granules. It is evident from several studies that the mean residence time (t_{m}) in a TSG (which is few seconds) is much shorter compared to the granulation time in a typical batch granulator, which is in the order of minutes. Although from a productivity point of view, this time gain

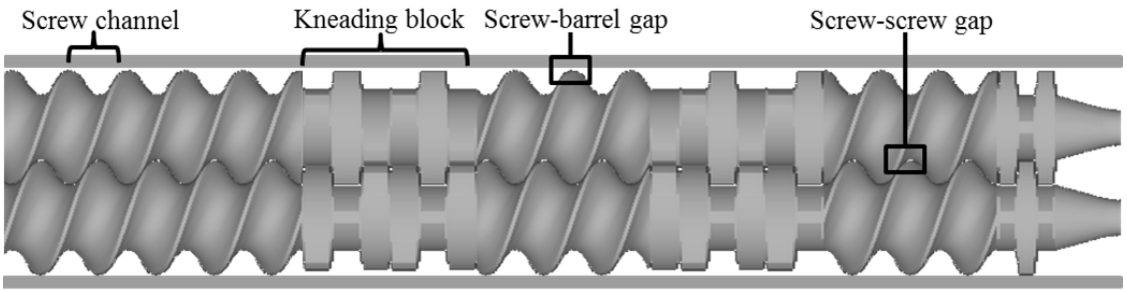

Figure 1: Screw configuration with 12 kneading discs (2 blocks) used in the twin screw granulator during the study.

is preferred, its implications on the granulation rate processes needs to be examined [2]. The mixing inside the granulator is related to the functional role of the screw configuration as well as process parameters. Feeding rates of the granulation material, the screw speed and the screw configuration can be independently chosen to yield desired mixing levels of the material.

In the high-shear environment of TSG, a good axial mixing in addition to the radial mixing during granulation in TSG is required to avoid the effect of any inhomogeneities at the inlet on the produced granules. A mixing region in a TSG screw contains blocks of several kneading discs with grooved flights, which cause a broadening of the residence time distribution (RTD). A broad RTD indicates good axial mixing in a TSG, and hence has a favourable effect on product quality by avoiding inhomogeneities in the final product. The RTD of the material is determined by the bulk flow profiles in the screw channels, generation of partial flows in flow-restrictive zones (e.g., in kneading blocks), and reverse flow in the gaps at the flight tips and in the inter-meshing zone as well as in mixing zones (Fig. 1). However, this leads to another optimization challenge regarding the most-suitable screw configuration.

In recent years, pharmaceutical continuous twin screw granulation has received increased attention and several researchers have investigated various aspects including the effect of key formulation variables [2–5] and screw configurations [6–8]. Similar to the regime map approach applied in batch wet granulation, an effort has been made to implement the regime map in TSG to predict a priori the response of the change in the process parameters on

the granule size distribution (GSD) characteristics [9]. The population balance equation (PBE) is a mathematical framework typically used for model-based analysis and to improve understanding of the HSWG process [10]. A better description of the flow properties within the granulator is required for an advanced PBE framework towards understanding the effects of the control variables in the TSG during granulation and track or predict the characteristics of the GSD produced as a function of space and time. Besides, the RTD exhibited by a given system yields distinctive clues regarding the type of axial mixing occurring within the system and is one of the most informative characterisation methods of the system [11].

Dhenge et al. [12] measured the RTD using the impulse-response technique under different processing conditions and showed the variation in the RTD depending on formulation and process parameters. El Hagrasey et al. [2] applied the same RTD measurement approach to estimate the response to changes in formulation properties such as raw material attributes as well as granulating liquid properties on granule properties. However, due to the difficulty to visualize the material flow in the barrel, little efforts have been made towards understanding the mixing of the material inside the TSG barrel, which is essential for the optimisation of the obtained granule properties. In a recent attempt, Lee et al. [13] obtained the RTD using positron emission particle tracking (PEPT) to study the axial mixing. Although this is a very powerful technique, this approach requires several manipulations in the equipment and the process (e.g. thinner TSG barrel wall to make sure that the gamma rays can penetrate the construction material, but it limits the shear handling capability of the barrel). Therefore, it would be beneficial to have a measurement method allowing RTD measurements without the need of manipulation of the equipment. Also, the PEPT involves single particle tracking, which is limited by the number of tracer passes to study the complete RTD adding operational variability to the RTD study. The circulated tracers in the PEPT study may not provide information on the total flow behaviour as some material paths are so rare that they will not be followed by the finite number of tracer paths through the equipment. Therefore, only distributions of passage time rather than true RTD can be measured using the PEPT [14]. Vercruysse et al. applied near infra-red (NIR) chemical imaging to evaluate the influence of the liquid addition method, screw configuration, moisture content and barrel

filling degree on the moisture homogeneity during TSG [15].

In this study, a novel sample preparation and an image data collection method based on NIR chemical imaging has been used as an analytical technique to characterise the flow and axial mixing of material in the TSG qualitatively and quantitatively. The study presented here examines the axial mixing inside a continuous TSG based on the characteristic RTD of the tracer component. NIR chemical imaging was used to investigate the residence time of tracer inside the barrel and its distribution as a function of process (screw speed and material throughput) and equipment parameters (number and stagger angle of kneading discs in screw configuration).

2. Materials and methods

2.1. Pharmaceutical formulation

α-Lactose monohydrate (Pharmatose 200M, Caldic, Hemiksem, Belgium) was used as a model excipient. Distilled water was added as granulation liquid. To evaluate the residence time of material inside the barrel, theophylline anhydrate (Farma-Química Sur, Malaga, Spain) was used as tracer component.

2.2. Continuous twin screw granulation

Granulation experiments were performed using a 25 mm diameter co-rotating twin screw granulator, which is the granulation module of the ConsiGma-25 unit (GEA Pharma Systems, Collette™, Wommelgem, Belgium). The granulator screw has a length-to-diameter ratio of 20:1. The TSG barrel consists of a feed segment, where the powder enters the barrel and is transported through the conveying zone to the work segment, where the granulation liquid is added to the powder which is further intensively mixed by a combination of kneading discs and transport screws [4, 5]. The barrel jacket was preheated to 25°C. During processing, pure α-lactose monohydrate was gravimetrically fed into the granulator by using a twin screw feeder (KT20, K-Tron Soder, Niederlenz, Switzerland). Distilled water as granulation liquid was pumped into the screw chamber by using a peristaltic pump (Watson Marlow, Cornwall, UK) and silicon tubings connected to 1.6 mm nozzles. The granulation

liquid was added (11.5% w/w) before the first kneading element (Fig. 1) by dripping through two liquid feed ports, each port located on the central top of each screw in the barrel. A shot of anhydrous theophylline (2% (w/w) of the material throughput) used as tracer was manually inserted into the powder inlet port of the granulator. The TSG has an inbuilt torque gauge and the steady state criteria were decided based on the equilibration of the measured torque of the granulator. The torque values obtained after equilibration of the process were averaged to give the overall torque during each run.

2.3. Description of NIR chemical imaging system and measurement setup

Spectral images of wet granules were collected using a line-scanning (pushbroom) hyperspectral camera (SWIR, Specim Ltd., Oulu, Finland). The camera sees a row of 320 spatial pixels at a time, and it disperses the incoming light from each pixel in the spectral range 970-2500 nm onto one column on the 320×256-pixel mercury-cadmium-telluride (MCT) detector (14-bit readout, cooled to -70°C with a 4-stage Peltier system). Wet granules from the granulator output fell on a conveyor belt (Mini, ENP, Hjälteby, Sweden) which was moving at a speed of 3.12 cm/s. The camera-to-belt distance was set such that the imaged line had the length of 10 cm on the conveyor belt, and the speed of the conveyor belt was adjusted such that the geometry was preserved, i.e., spatial pixels were squares of the size 312×312 μm^2 at the maximum frame rate permitted by the camera (100 frames per second). The conveyor belt and the sample material on it were illuminated with two rows of three 75-W halogen lamps (Specim Ltd., Oulu, Finland) at the distance of 35 cm, and the measurement was conducted in diffuse reflectance mode in the 45°-0°-45° geometry (see Fig. 2). Each collected spectral image consisted of 2500 frames (25 seconds measurement, 2500×320 spatial pixels, 256-element spectrum at each spatial pixel) which corresponds to an area of 10×64 cm^2 on the conveyor belt. At the material throughput of 10-25 kg/h the dry mass of material in one spectral image was approximately 69-173 g.

Extraction of relevant information from chemical images

The processing of the hyperspectral images consisted of two steps. First, spatial pixels corresponding to the plastic conveyor belt were eliminated from the analysis via partial

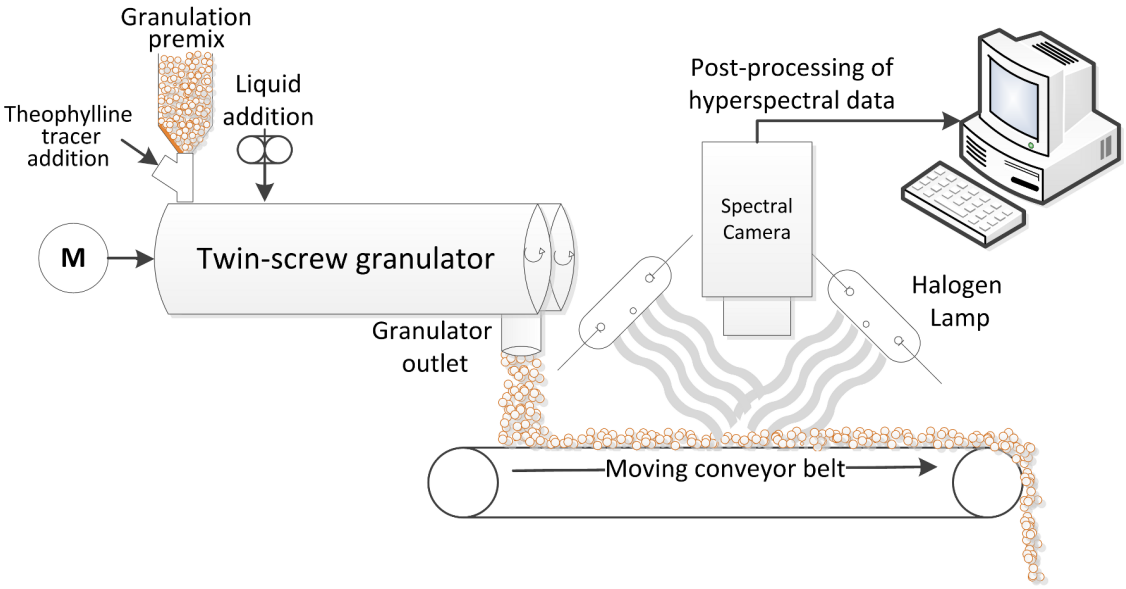

Figure 2: Schematic diagram of the measurement setup at the outlet of the granulator. Granules at conveyor belt moving at constant speed were illuminated using the halogen lamps and scanned by the spectral camera.

least squares discriminant analysis (PLS-DA) classification. Second, the NIR spectra in the remaining pixels corresponding to the wet granules were subjected to semi-quantitative analysis of theophylline content. The spectral range was narrowed to 1100-2200 nm and the spectra were subjected to the standard normal variate (SNV) pretreatment in all analyses. The use of SNV preprocessing eliminates the additive baseline offset variations and multiplicative scaling effects in the spectra which may be caused by shadowed regions near large granules and possible differences in granule density. Both steps have been described in detail by Vercruysse et al. [15].

2.4. Residence time analysis: experimental design and data post-processing

2.4.1. Experimental procedure to collect raw data

Experiments were performed to study the influence of screw speed (500, 700, 900 rpm), material throughput (10, 17.5, 25 kg/h), number (2, 6, 12) and stagger angle (30, 60, 90°) of the kneading discs in the screw configuration on the RTD and axial mixing of the material. For the different experiments, pure α-lactose monohydrate was fed to the granulator. The screw configuration was composed of kneading zones consisting of maximum 6 kneading

discs in each zone (L = $^{D}/_{4}$ for each kneading element) at an angle of 30, 60 and 90 degrees (Fig. 1). Both kneading zones were separated by a conveying element (L = 1.5 D). An extra conveying element (L = 1.5 D) was implemented after the second kneading block together with 2 narrow kneading discs (L = $^{D}/_{6}$ for each kneading element) in order to reduce the amount of oversized agglomerates, as reported by Van Melkebeke et al. [6]. The granulation liquid (liquid to solid ratio 10% (w/w) of the material throughput) was added just before the first kneading element.

During each experiment, a shot of anhydrous theophylline (2% (w/w) of the material throughput per minute, which corresponds to 3.33, 5.83 and 8.33 g for throughput of 10, 17.5 and 25 kg/h respectively) was manually inserted into the powder inlet port of the granulator. At the outlet of the granulator, the NIR chemical imaging system was used to measure the theophylline dynamics. The chemical imaging measurements were started 5 s after the addition of the theophylline shot. Since it took 5 s for the conveyor belt to move from below the granulator output to the location of the spectral image collection (Fig. 2), the first frame of the spectral image corresponded to the instant of theophylline addition. The spatial distribution of theophylline during the 25 seconds measurement was calculated with the spectral matched filter as explained in section 2.4.1. The intensity of the obtained chemical map was thus proportional to the true theophylline level, and the residence time distribution could be determined via inspecting the temporally scanned direction of the spectral image. For each residence time analysis experiment, a semi-quantitative measure of the theophylline level was obtained using the previously described method by Vercruysse et al. [15].

2.4.2. Estimation of RTD and axial mixing efficiency

Conventionally, a residence time distribution is obtained by injecting a pulse of tracer into the system at the inlet, and the residence time function, $e(t)$, is calculated as

$$e(t) = \frac{c(t)}{\int_0^\infty c(t)dt} \tag{1}$$

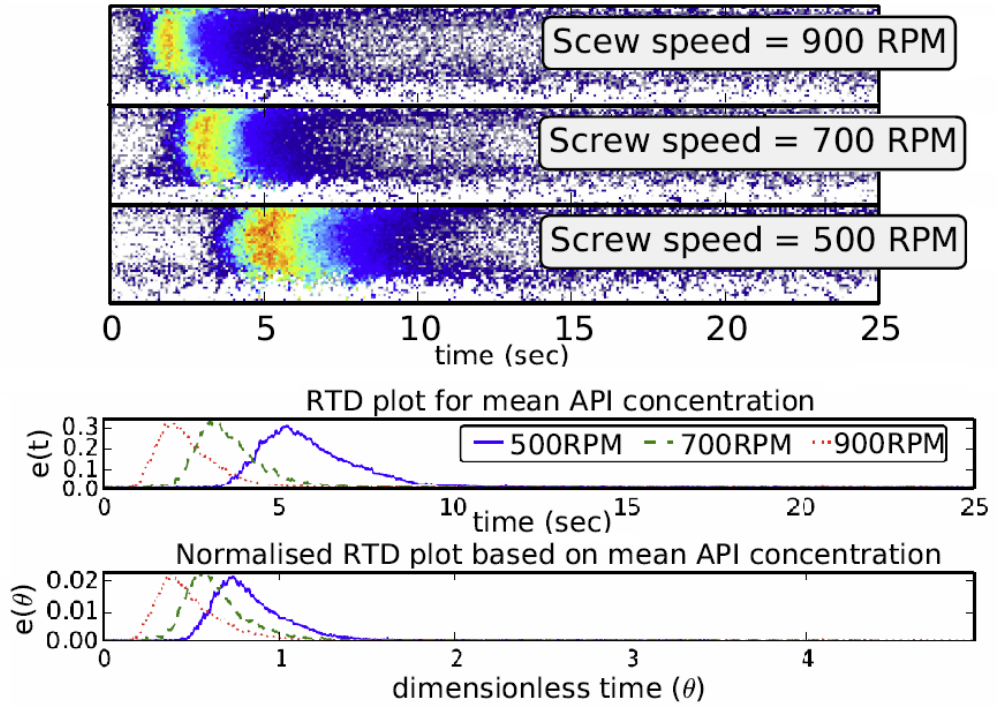

Figure 3: Representation of active pharmaceutical ingredient (API)-map, corresponding temporal profile and residence time distribution for twin screw granulator at fixed material throughput (25 kg/h), number of kneading discs (6), stagger angle (60°) and different screw speeds

where $c(t)dt$ is the concentration of the tracer at the outlet between t and $t + dt$. In this study, the residence time of the tracer molecule (theophylline) was applied as the function of the tracer concentration (as estimated with the SMF model) between t and $t + \delta t$ in the temporal profile of the discrete tracer map (top of Fig 3). This tracer map was transformed into the exit age distribution curve, i.e. RTD based on the mean tracer concentration, e(t) between t and $t + dt$ (middle plot of Fig 3), which was then used to calculate the mean residence time (t_{m}) as the ratio of the first and the zeroth moment using equation

$$t_m = \frac{\int_0^\infty t.e(t)dt}{\int_0^\infty e(t)dt} \tag{2}$$

The RTD shape, thus obtained was normalised (bottom plot of Fig 3) as $e(\theta) = t_m.e(t)$, where dimensionless time, $\theta = {}^{t}/_{t_m}$, and used to characterise the axial mixing levels. The degree of axial mixing in the granulator can be quantified by calculating a dimensionless Péclet number (Pe) which is a ratio of rate of axial transport by convection and axial

transport by diffusion or dispersion. By treating the boundary condition of the granulator as a closed system with no dispersion or radial variation in concentration either upstream or downstream, the following equation can be derived [16]

$$\frac{\sigma_{t_m}^2}{t_m^2} \approx \frac{2Pe - 2 + 2 \cdot e^{-Pe}}{Pe^2} \tag{3}$$

where, the mean centered variance ($\sigma_{t_m}^2$), which measures the width of the RTD, is calculated by

$$\sigma_{t_m}^2 = \frac{\int_0^\infty (t - t_m)^2 . e(t) dt}{\int_0^\infty e(t) dt} \tag{4}$$

and the $\sigma_{t_m}^2/t_m^2$ in eq. 3 stands for the normalised variance (σ_θ^2), which is the normalised second central moment of the RTD curve. As $\sigma_{t_m}^2$ approaches zero, Pe approaches infinity indicating that the extent of axial mixing is low. When the Pe turns out to be large, the granulator characteristics approach those of a plug-flow reactor (PFR). This regime is not favourable in continuous processing as the existence of plug flow indicates poor axial mixing in the granulator which is not desirable.

2.5. Quantification of effects and interactions of factors

The data collected by the experimental design were used to estimate the effects of the factors on the responses. Since, multiple responses (t_m, σ_θ^2, Pe) were quantified from the RTD profile, it was helpful to fit a model simultaneously representing the variation of all responses to the variation and interaction of the factors. Therefore, using Modde 9.0 software (Umetrics, Umeå, Sweden), the partial least squares (PLS) method which is able to deal with many responses simultaneously, taking into account their covariances, was employed. The effect plot was used to show the change in the response when a factor and its combinations vary from low level to high keeping other factors at their averages (Fig. 5). The respective 95 % confidence interval is shown for each plot. Insignificant effects are those where the confidence interval includes zero. The interaction plot has been used to display the predicted change in the response when one factor varies, and the second factor is set at both its low

and high level, all other factors being set on their center. In this plot, when the two lines are parallel there is no interaction between the two factors, whereas when they cross each other there is a strong interaction.

3. Results and discussion

Residence time analysis of the tracer molecule (theophylline) was performed as a function of material throughput, screw speed, and screw configuration in terms of number and stagger angle of kneading discs (see overview of performed experiments in Fig. 4). The curves based on the exit tracer concentrations display a long tail for all the runs (Fig. 4), which indicates that the flow behaviour inside the granulator is not plug flow under the conditions used in this study and that a significant degree of axial mixing occurs. This was also demonstrated by El Hagrasy et al. in a study for RTD in a TSG [2]. Besides changes in RTD profile, the effect of these process and screw design parameters clearly reflected in other responses such as measured torque in the granulator drive (Fig. 6), the mean residence time (t_{m}) (Fig. 7), width of the normalised RTD i.e. normalised variance (σ_{θ}^{2}) (Fig. 8) and relative magnitude of convective and dispersive transport capacities (Fig. 9) in the TSG. This now allows discussion of the effects of each factor and their interactions based on their RTDs and the axial mixing of the material (Fig. 5). In what follows the observed effects are discussed in more detail.

3.1. Effect of screw speed

Screw speed had the largest effect on the RTD indicating that a highly frictional flow exists and thus the TSG behaves dominantly like a drag pump (Fig. 5). With the increase in screw speed the RTD profiles consistently shifted to the left in Fig. 4, suggesting a decrease in the t_{m} of the material in the TSG barrel. This is expected as the conveying rate increases with the increased screw speed, which reduces the residence time of the material in the granulator. At lower filling conditions (i.e. low material throughput and low number of kneading discs) the difference between the RTD profiles at higher screw speed (900 and 700 rpm) was less compared to that at low screw speed (500 rpm). With the increase in

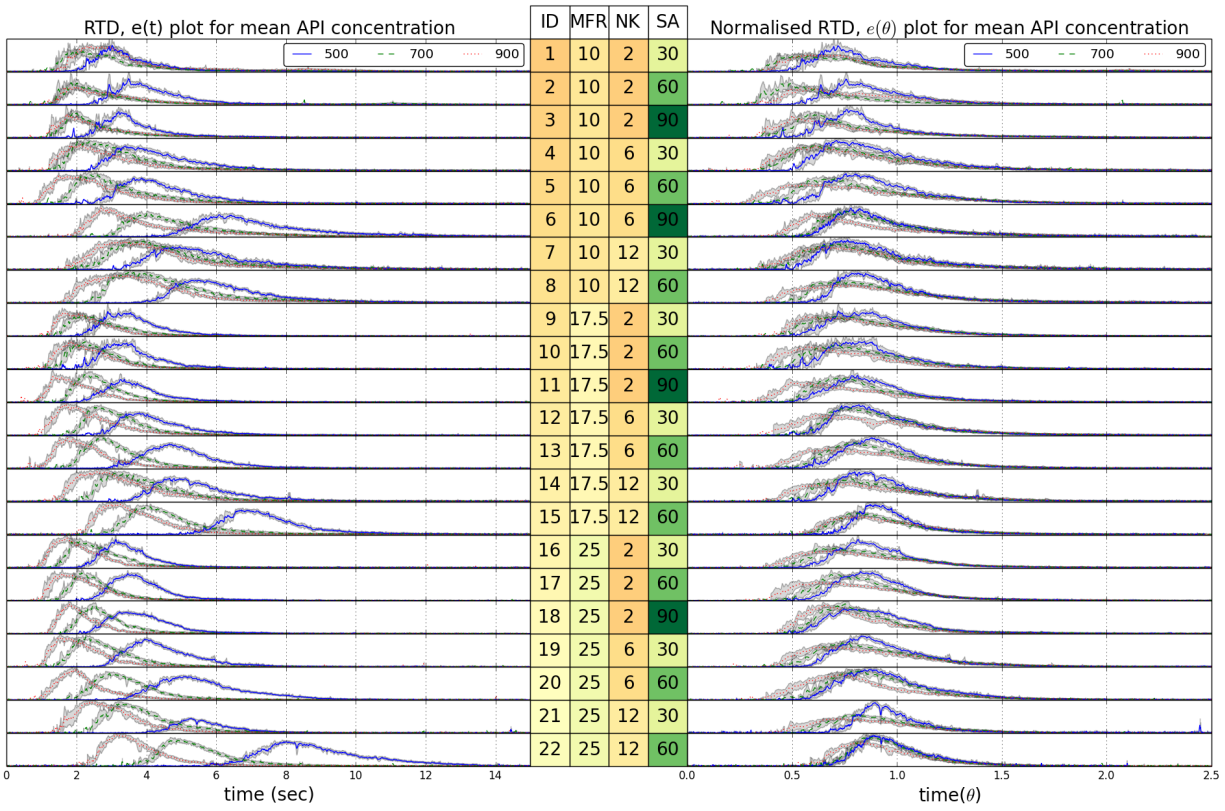

Figure 4: The age distribution (left) and normalised RTD (right) profiles with a shaded region denoting the standard deviation at different screw speed (500, 700, 900 RPM) during various experiments (ID) using twin screw granulation [SA: stagger angle (°), NK: number of kneading discs (-), Mfr: material throughput (kg/h)]. Several RTD profiles for experimental runs at SA = 90° are not shown as the TSG barrel jammed for those conditions.

material throughput, the fill ratio was high enough to induce a difference between RTDs at all screw speeds (right side plots with ID 9-22 in Fig. 4). This difference became larger with an increase in the number of kneading discs (such as ID 12 and 14 compared to ID 9 in Fig. 4) and their stagger angle (ID 16, 17 and 18 in Fig. 4). At low screw speed (500 rpm) significant variation in the RTD was observed between different screw configurations and the mean exit tracer concentration in the active pharmaceutical ingredient (API) maps were detected between 4.1 and 8.6 seconds after injection of the API shot. In contrast, at high screw speed this difference reduced and the mean values of the tracer concentration in the API maps were detected between 2.8 and 4.6 seconds after injection of the API shot. This reduction indicates that the increase in the screw speed leads to a reduction in the influence of other factors under study.

These changes in RTD profile due to changes in screw speed also affected other responses. At a high number of kneading discs, the torque decreased significantly with an increase in screw speed in contrast to the low number of kneading discs (Fig. 6). This is due to the increased conveying rate at high screw speed, which reduced fill level of the powder accumulated by a high number of kneading discs [12]. The reduced fill level resulted in reduction in the torque level. The t_{m} as well decreased with an increase in the screw speed (Fig. 7). However, the difference between t_{m} was smaller when the screw speed was increased from 700 to 900 rpm compared to an increase from 500 to 700 rpm. The change in screw speed also affected the σ_{θ}^{2} (eq. 4), which generally increased with an increase in the screw speed (Fig. 8). However, at the high filling condition (material throughput 25 kg/h, 12 kneading discs), the effect of screw speed on the σ_{θ}^{2} was the least. This was due to material built up at the two kneading blocks in the TSG, which ensured near-plug flow conditions inside the TSG. An additional conveying cleared the kneading blocks, but could only lead to a minor increase in axial mixing.

An increase in the screw speed resulted a reduction in Pe reflecting that dispersive transport was high compared to the convective transport in the TSG (Fig. 9). At lower screw speed, Pe increased significantly with an increase in throughput, number of kneading discs and stagger angle, indicating low axial mixing and more plug flow like material transport

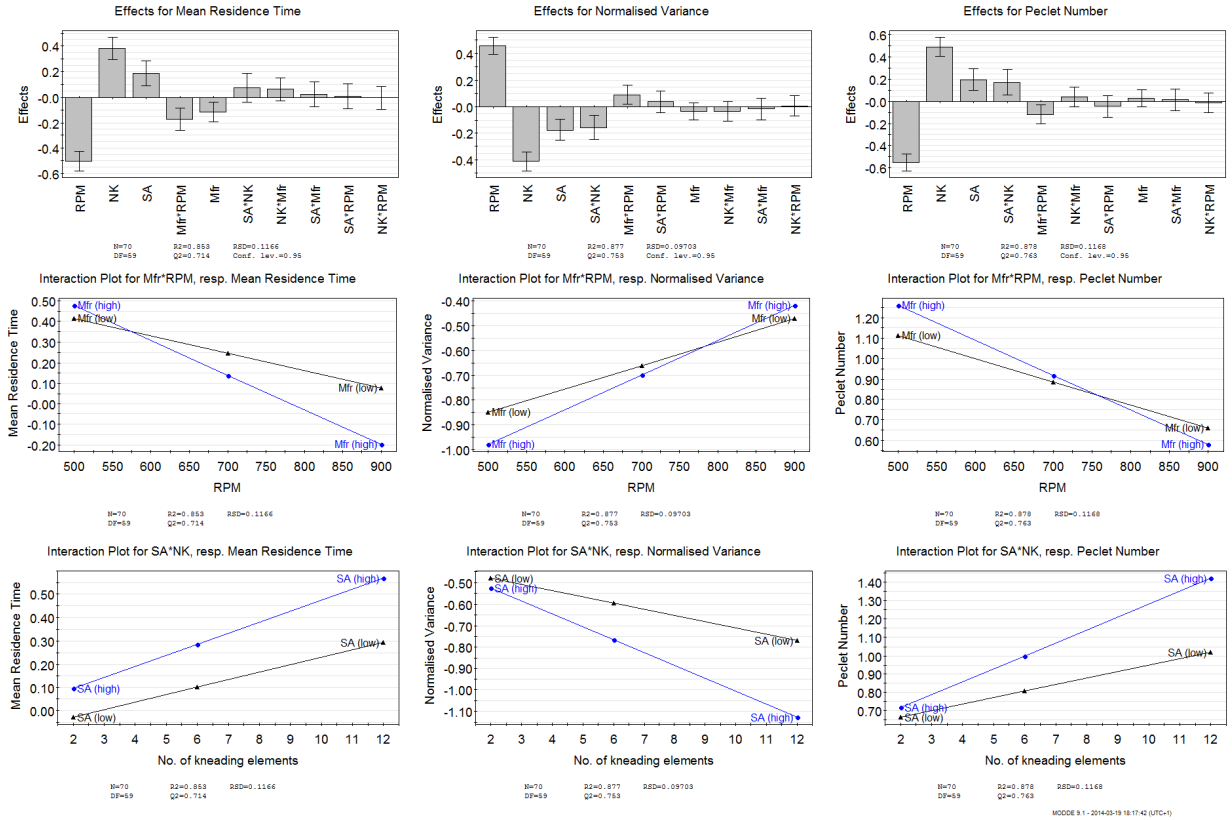

Figure 5: Effects and related interaction plots of the partial least squares (PLS) models showing change in the responses in term of mean residence time, normalised variance, Péclet number and the measured torque when factors number of kneading discs (NK) [2, 6, 12], screw speed (RPM) [500-900 rpm], throughput (Mfr) [10-25 kg/h] and stagger angle (SA) [30-90°] and their interaction varies from average to the high level.

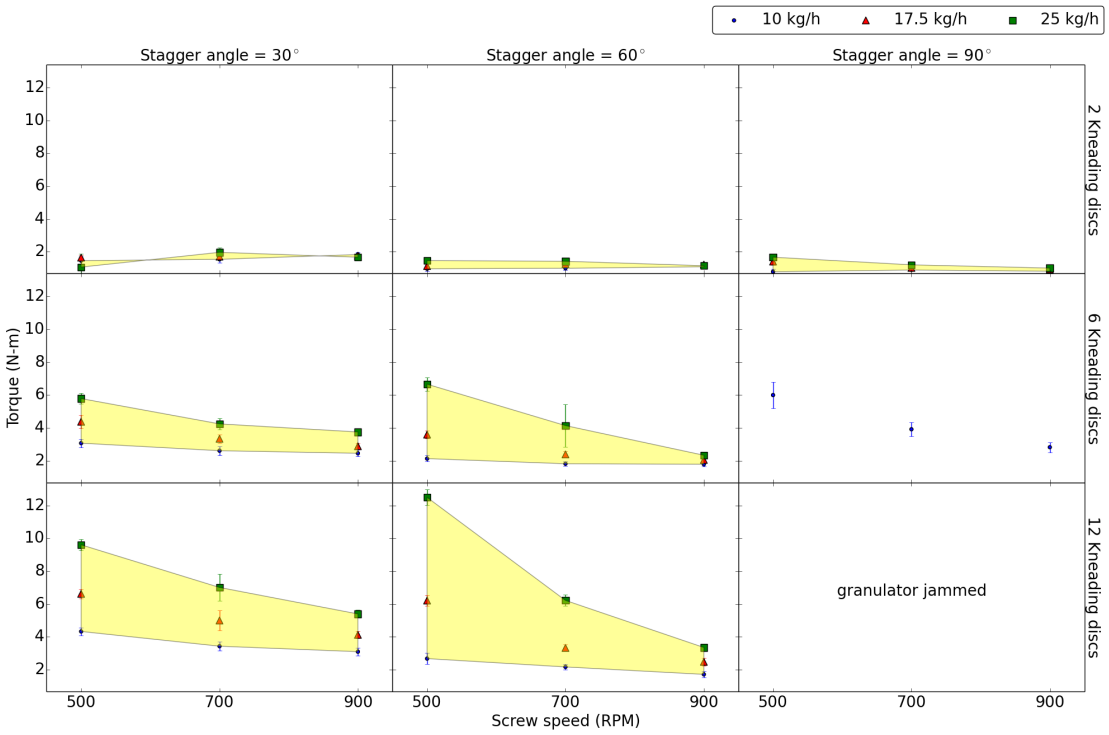

Figure 6: Average torque measured and the standard deviation at various material throughputs (10-25 kg/h), number of kneading discs (2, 6, 12), stagger angle (30-90°) and different screw speeds (500-900 rpm)

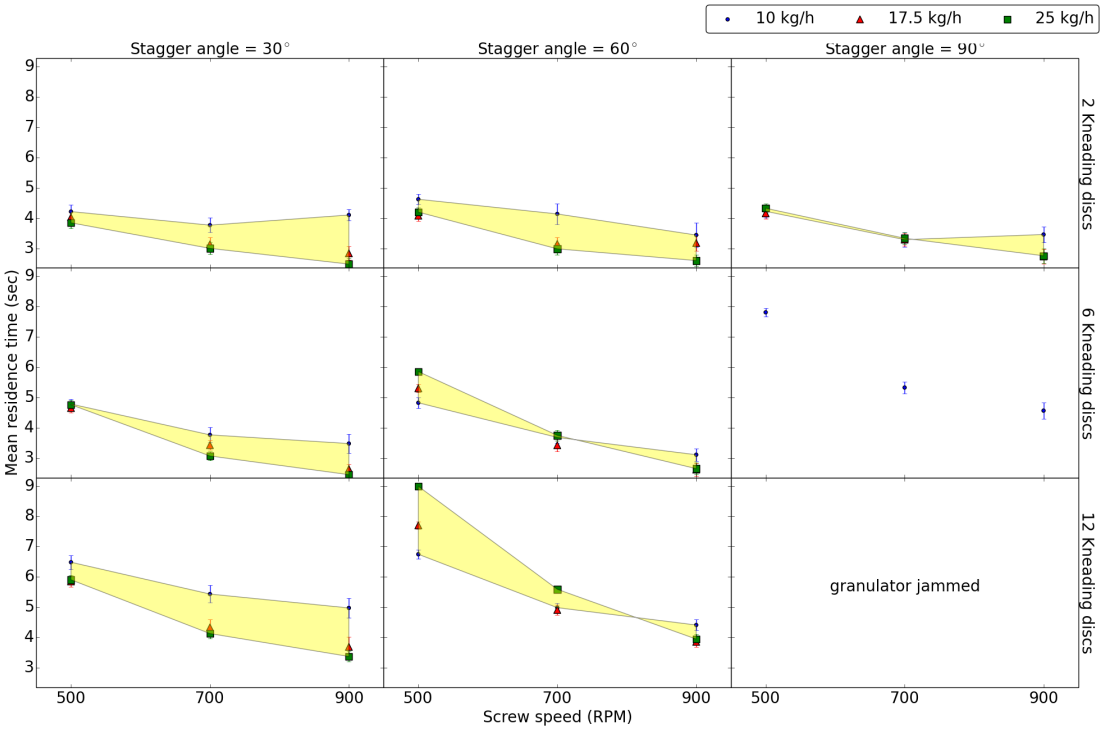

Figure 7: Mean residence time (t_{m}) and the standard deviation based on the experimental RTD profile at various material throughputs (10-25 kg/h), number of kneading discs (2, 6, 12), stagger angle (30-90°) and different screw speeds (500-900 rpm)

through the barrel. The high Pe was possibly due to the bulk movement of material in lack of critical strain and homogenisation force. These results contradict the findings by Lee et al. [13] who suggested more effective axial mixing at lower screw speed as the particles got stuck in the restrictive zones (kneading blocks) more frequently at lower screw speed than at higher screw speed. However, the study by Lee et al. [13] was performed using screws of lower diameter (16 mm) and at lower screw speed (200-500 rpm). This contradiction can be understood by the results of Gautam and Choudhury [17] who reported that the extent of the axial mixing in the twin screw extruder is significantly affected by the screw types and screw geometries. We believe that possibly due to the small clearance between the two screws and the wall in the TSG used here, the reverse-flow was significantly prevented at lower screw speed in this study, which led to a completely different outcome. The material layering on the barrel wall leading to a reduction in the clearance gaps may also be responsible for this lack of reverse-flow at low screw speed.

3.2. Effect of material throughput

The fill degree which dictates the level of axial mixing in TSG is also controlled by the material throughput. However, the effect of throughput was less significant without interaction with other factors (Fig. 5). When the flow in the TSG barrel was less of a constraint (stagger angle of 30 and 2 kneading discs, screw speed 900 rpm), increasing material throughput had no significant effect on the RTD. When the restrictive forces increased (through changes in screw configuration), despite low fill ratio at low throughput, the RTD profile shifted to the right (left side plots with ID 4-8 in Fig. 4), indicating an increase in the residence time of the material in the TSG barrel. As the fill ratio was increased by the increase in the material throughput, the RTD shifted also at lower restrictive forces (left side plots with ID 9-11 and 16-18 in Fig. 4). The high material throughput caused a higher degree of channel filling of the screws, creating a high throughput force. The shortest time for detecting the mean values of the tracer concentration in the API maps was 2.8 sec (left side plot ID 16 in Fig. 4) at a material throughput of 25 kg/h at 900 rpm. This might be due to very high throughput force which conveyed the material quickly. However, this shift in RTD did not always translate into an increase in the axial mixing. At the low material throughput the degree of channel filling is low, hence there is a low throughput force of the material, which can lead to more axial mixing [18]. This is also visible in the trends in the study (right side plots with ID 1-8 in Fig. 4). But, when the material throughput increases beyond the conveying capacity of the screw, it may have resulted in plug flow of the material leading to poor axial mixing as indicated by reduction in width of the distribution (comparing right side plots with ID 8, 15 and 22 in Fig. 4).

The torque profile was less affected by the change in the material throughput when restrictive forces were less i.e. at the low number of kneading discs, low stagger angle and high screw speed (Fig. 6). However, with an amplification of restrictive force, the torque changed significantly for changes in the material throughput. At the screw speed of 500 rpm, 12 kneading discs and stagger angle of 60°, the maximum change in the measured torque, from 2.7 Nm to 12.5 Nm for increase in material throughput from 10 kg/h to 25 kg/h, was observed (Fig. 6). When the screw speed was increased, the measured torque decreased

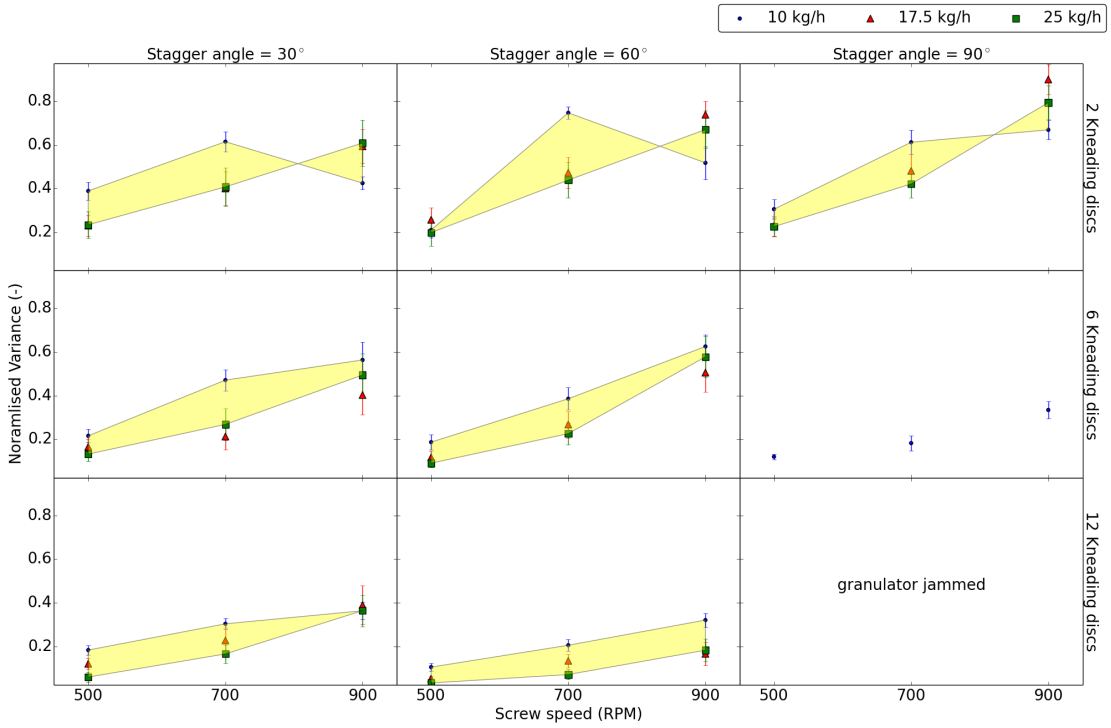

Figure 8: Normalised variance and the standard deviation based on the experimental RTD profile at various material throughputs (10-25 kg/h), number of kneading discs (2, 6, 12), stagger angle (30-90°) and different screw speeds (500-900 rpm)

significantly due to higher thrust of the material by the rapidly moving screws.

An increase in the conveying rate with increasing material throughput also caused reduction in the t_{m} (Fig. 7). However, at low screw speed (500 rpm), the t_{m} increased with increasing material throughput for the screw configuration with 6 kneading dics at stagger angle of 60°. This indicates lack of possibility to push forward more material to create extra conveying capacity for this screw configuration, thus causing higher restriction to flow and increase in the t_{m}. For the screw configuration with 30° stagger angle, at high screw speed (900 rpm), the difference in t_{m} was relatively higher for an increase of the material throughput from 10 to 17.5 kg/h compared to the difference observed when increasing from 17.5 to 25 kg/h. This suggests that extra conveying capacity cannot be achieved constantly by an increase in the material throughput. In contrast, at 60° screw configuration, the material throughput had a larger impact on the t_{m} at lower screw speed (500 rpm), which decreased with increase in screw speed. This can be regarded as a requirement of critical fill ratio to be

achieved for each screw configuration to extend the t_{m} and change the overall RTD profile.

Although, the effect of change in the material throughput on σ_θ^2 and Pe was observed to be insignificant by the PLS model when considered alone (Fig. 5), the general trend shows a reduction in σ_θ^2 with an increase in the material throughput (Fig. 8). This was due to the increased throughput force, which led to an increase in compaction and reduction in the wall slippage, and hence the reduced axial mixing in the TSG. Similarly, an increase in Pe was observed when the material throughput was increased (Fig. 9). This suggests that the convective transport dominates over dispersive transport with an increase in the throughput. At the highly restrictive flow condition (12 kneading discs at 60°), the increase in the material throughput led to convective transport outcompeting dispersive transport leading to very high Pe. Therefore, the material flow in the barrel approaches a plug flow regime. The materials in the TSG with a low degree of filling could be less compacted than those in the TSG with a high degree of filling. This led to greater axial transport in the TSG. However, the number of kneading discs and their stagger angle dominated the control of the residence time, which resulted in complete jamming of the granulator at high material throughput, more kneading discs (12) and stagger angle (90°). Hence, a balance between conveying and dispersive forces is required to obtain the desired axial mixing and residence time while changing the material throughput.

3.3. Effect of number of kneading discs

Next to the screw speed, the number of kneading discs was a significant factor having effect on the RTD characterstics without interaction with other factors (Fig. 5). In a TSG, the fed material is only rolled forward by the conveying section. A significant mixing occurs in the mixing section since the material in this section flows more slowly than in the previous conveying section and is, hence, forced-mixed with the incoming materials. Thus, it is an important factor in RTD studies for TSG. The influence of kneading discs is primarily reflected by the increase in the driving torque of the TSG with an increase in the number of kneading discs (Fig. 6). At a low number (2 kneading discs) for all different screw speeds, material throughputs and stagger angle of the discs the torque was below 2 Nm. However,

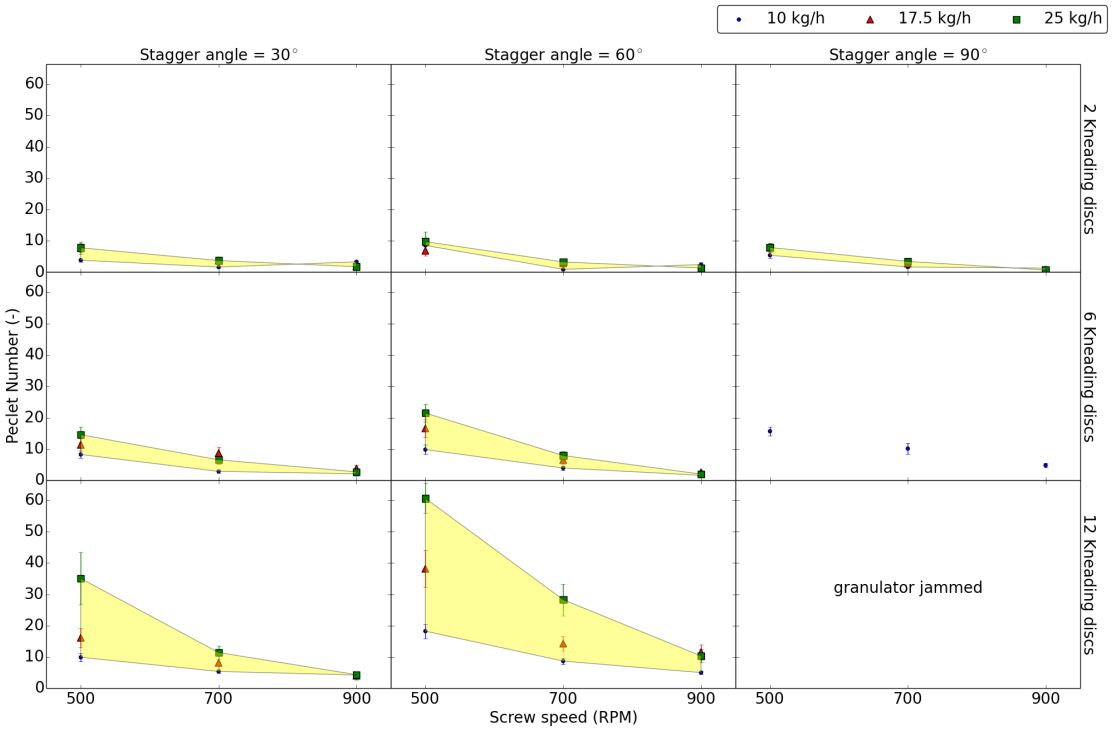

Figure 9: Peĉlet number (Pe) and the standard deviation based on the experimental RTD profile at various material throughputs (10-25 kg/h), number of kneading discs (2, 6, 12), stagger angle (30-90°) and different screw speeds (500-900 rpm)

by increasing the number of discs, the torque value increased to a level as high as 10 Nm. For low screw speed (500 rpm) and high stagger angle (60°), the restrictive forces started to dominate over drag force in the mixing zone, which caused an excessive increase in the torque of the granulator. For a higher number (6 and 12) of kneading discs and stagger angle (90°) the flow of material was so seriously hampered that the TSG barrel jammed and the run could not be performed. Next to the measured torque, this increase in restrictive flow was clearly reflected in the RTD (Fig. 3). With an increase in number of kneading discs the RTD shifted towards the right in the experiments with ID 17, 20 and 22 of Fig. 4, indicating an increased restriction to the flow of material in the TSG barrel. However, the difference between the RTD profiles for experiments with screw configuration consisting of 2 and 6 kneading discs was smaller compared to the difference observed when shifting between 6 and 12 kneading discs. This may be explained by the fact that up to 6 kneading discs there was only one kneading block in the screw while in the case of 12 kneading discs an additional kneading block containing 6 kneading discs was present. In a TSG with more than six kneading discs, the material has to travel consecutively through a conveying section, a mixing section, again a conveying section and finally a mixing section before being conveyed out.

The increase in number of kneading discs caused an increase in t_{m} of the tracer, which was well expected due to increase in flow restriction (Fig. 5). Consequently, the local fill level was increased, leading to a material consolidation, until it was expelled to the next section i.e. kneading section [9]. While the number of kneading discs had little impact on the t_{m} at high screw speed (900 rpm), this becomes significant at lower screw speeds (500, 700 rpm) leading to a high t_{m} (Fig. 7). At a low number of kneading discs, the t_{m} was found to be in a lower range (3 - 5 sec) compared to the result obtained for 12 kneading discs (4 - 9 sec). Contrary to t_{m}, the σ_{θ}^{2} is most influenced at the low number of kneading discs (Fig. 8). Due to low hindrance to the axial flow by the shortest fully filled zones around two kneading discs, dispersive transport was most efficient. Also, since flow restrictive influence by kneading discs was the least, the impact of other factors on the axial mixing was more expressed. On the other hand, at the high number of kneading discs excessive hindrance

causes a quick shift towards plug flow, which was supportive of other flow restrictive factors such as, low screw speed (500 rpm) and high stagger angle (90°). Therefore, less variation in the σ_θ^2 was observed at the high number of kneading discs despite changes in other factors under study. The relative magnitude of the convective to dispersive transport capacities showed that the convective transport dominates over dispersive transport with increase in number of kneading discs (Fig. 9). At a low number of kneading discs the Pe was between 2 - 12, while for a screw configuration involving 12 kneading discs, screw speed 500 rpm and material throughput of 25 kg/h the Pe increased up to 45. Increasing the screw speed up to 900 rpm for the same condition reduced the Pe rapidly up to 10.8. Such a behaviour shows that, at a higher number of kneading discs, although the t_m is increased in the TSG barrel, an increase in screw speed is required to achieve proper axial mixing.

3.4. Effect of stagger angle

Change in stagger angle had significant effect on the RTD characteristics of the TSG (Fig. 5). However, since the restricted area in the flow channel of the TSG is small per kneading disc, the impact of the stagger angle on the RTD profile is only observed with an increased number of kneading discs. This is due to an additive restriction of the flow at a higher number of kneading discs. Thus, a cumulative effect by increasing number and stagger angle of kneading discs caused an increase in the driving torque of the TSG (Fig. 6). At low number of kneading discs, despite changes in stagger angle of the kneading discs, the measured torque of the TSG drive was always below 2 Nm. However, with an increase in the number of discs, the torque value showed variation at different stagger angles and later on became such a dominant factor that several runs at 90° stagger angle could not be performed due to jamming of the TSG barrel. This can be attributed to the excessive restriction to the material flow at the high number of kneading discs and a lack of thrust to flow at a stagger angle of 90°. This increased constrained flow shifted the RTD profile to the right with increasing stagger angle (left side plots with ID 4-8, 12-15 and 19-22 in Fig. 4). However, this shift did not always contribute to an increase in width of the distribution, an indicator of axial mixing. For the runs with 6 kneading discs and throughput of 10 kg/h,

an increase in stagger angle from 30° to 60° led to widening of the distribution, but further increase to 90° caused narrowing of the distribution (right side plots with ID 4-6 in Fig. 4). This can be explained by transition from a less-mixed to a well-mixed and later towards a plug flow profile in the TSG. Similar trends were observed for 12 kneading discs (right side plots with ID 7-8 in Fig. 4) as well as increased material throughput (25 kg/h) (right side plots with ID 21-22 in Fig. 4). Furthermore, at 2 kneading discs, only when the barrel was highly filled due to high material throughput (25 kg/h), the normalised RTD profile became wider when the stagger angle changed from 30° to 60° and no narrowing of the profile occurred even for an increase up to 90° (right side plots with ID 16-18 in Fig. 4). This indicates that stagger angle does play a significant role in axial mixing.

A change in stagger angle affected the t_{m} more clearly at 6 and 12 kneading discs and low screw speed (500 rpm) (Fig. 7). The t_{m} became higher and the material spent an extra 2 to 3 seconds in the TSG barrel. The increase in t_{m} was presumably due to the increased restriction and reduced conveying capacity of the 60° kneading discs, compared to that of the 30° configuration. The t_{m} using the 90° kneading block configuration was higher than for the 30° and 60° configurations. The material was observed flowing through the granulator at the low number of kneading discs (2 and few runs with 6 kneading discs) and blocked completely for 12 kneading discs at 90°. A mixing zone with 90° kneading discs arrangement in principle gives no conveying capacity [13]. Hence, it can be suggested that the material transport through the mixing zone occurs largely due to the throughput force and the gradient of filling degree along the granulator, and is strongly coupled with the material throughput and the screw speed. The stagger angle had a significant effect on the axial mixing, which is reflected by a reduction in σ_{θ}^{2} with an increase in stagger angle (Fig. 5). This reduction in σ_{θ}^{2} suggests that the stagger angle increase not only stimulates the reduction of the downstream conveying action of the screw but also impedes the axial dispersion in the granulator (Fig. 8). The less variation in Pe upon change in stagger angle at high screw speed (900 rpm) (Fig. 9) suggests that stagger angle has less effect when the dispersive transport dominates (low Pe) in TSG. However, at low screw speed along with an increase in feed rate, convective transport dominated over dispersive transport (high Pe).

An extremely significant effect of the change in stagger angle on the Pe was observed for 6 and 12 kneading discs where the Pe almost doubled with the increase in the stagger angle from 30° to 60°. Most of the runs for the screw configuration involving 90° stagger angle could not be performed as the flow regime moved to almost pure plug flow due to which the granulator jammed.

4. Interaction of different process and equipment parameters

The mixing and transport of the material in the TSG shows interactions between screw design, materials throughput and process parameters (Fig. 4). Thus, a combination of these parameters can be used to achieve a further increase in the t_{m} and the axial mixing reflected by the increase in σ_{θ}^{2} and set a balance between convective and dispersive transport in the TSG barrel. The strongest interaction occurred between the screw speed and the material throughput. Although increasing either screw speed or the throughput caused a reduction in t_{m}, their combined effect was less than expected due to their interaction (Fig. 5). Physically, the high level of throughput leads to a higher fill degree in the barrel and hence increase in restriction to the material flow. In such condition increasing screw speed can cause a lower reduction in t_{m} than low fill condition. The screw speed and the material throughput interaction was also strong in case of σ_{θ}^{2} and Pe, where the material throughput with insignificant effect became significant upon interaction with the screw speed (Fig. 5). This was mainly due to the interaction between the decreasing screw speed and increasing material throughput, which caused material accumulation in the TSG barrel and the material flow became a dense phase plug flow system, hence leading to reduced σ_{θ}^{2}. Increasing screw speed and resulting higher shear in the barrel results in increased σ_{θ}^{2} due to the change in the shear-slip velocity relation. As there is a clearance between the wall and the screw, a thin layer of material is expected to be formed on the barrel wall. This thin layer of material is not stationary, but slips slowly in the positive direction due to the high shear at higher screw speed [13]. Particles from this slow moving layer of granulation material will escape to the bulk flow of the material under the high shear force induced by the rotating screws. At the same time, particles in the normal flow stream may also

be trapped in the slow moving thin layer. This phenomenon is anticipated to happen more when the screw speed was increased, subsequently increasing the axial mixing as observed in this study. This change in flow system was also responsible for the inversion of the relation between the convective and dispersive transport with changing screw speed and throughput as reflected by the interaction plot for the Pe in Fig. 5.

The second important interaction occurred between the number and stagger angle of kneading discs. Although for t_{m} this interaction was insignificant, a mild interaction was observed for the σ_{θ}^{2} and the Pe (Interaction plot for σ_{θ}^{2} and Pe in Fig. 5). This happens mostly due to the strong dependence of the stagger angle on the number of kneading discs. Since the kneading discs in the mixing zones do not avail conveying capacity, material bypassing occurs more regularly in the transport screw zone and mixed flow regime. Thus, when the number of kneading discs and stagger angle are increased simultaneously it leads to reduction in material bypassing and less axial mixing in the TSG barrel.

Therefore, it can be stated that along with the process parameters, the configuration and geometry of the screw and the circumferential clearance between the screws and between screw and wall have a key role to play in this process. However, more work is needed to validate this hypothesis and to obtain more data for the investigation of the RTD tail. Furthermore, the results obtained from this study require to be linked to the granules characterisation study. Together with such a study it can be confirmed which mixing regime is most desirable for the granulation purpose.

5. Conclusions

NIR chemical imaging was shown to be an adequate tool for residence time analysis as representative and fast measurements could be obtained. Increased screw speed led to a lower t_{m} and narrower residence time distribution. According to the study, the variations of screw rotation speed, material throughput, number of kneading discs and stagger angle not only have a direct influence on the residence time of the material feed but also on the axial mixing during granulation using TSG. It seems that the screw geometry was one of the important factors affecting the axial mixing. This study has shown that changes in experimental

conditions can lead to very different flow regimes, and it is an oversimplification to say that twin-screw granulator shows a plug flow mixing characteristic. The results obtained in this study will be used in future work for linking mixing and transport characteristics in TSG to the particle characterisation study and develop a mathematical model for the continuous granulation considering both mixing and granule characteristics.

Acknowledgements

Financial support for this research from the BOF (Bijzonder Onderzoeksfonds Universiteit Gent, Research Fund Ghent University) is gratefully acknowledged.

Acronyms

$\sigma^2_{t_m}$ mean centered variance

σ^2_θ normalised variance

$\boldsymbol{t_m}$ mean residence time

API active pharmaceutical ingredient

GSD granule size distribution

HSWG high shear wet granulation

NIR near infra-red

PBE population balance equation

Pe Péclet number

PEPT positron emission particle tracking

PFR plug-flow reactor

PLS partial least squares

PLS-DA partial least squares discriminant analysis

RTD residence time distribution

SNV standard normal variate

TSG twin-screw granulator

References

[1] C. Vervaet, J. P. Remon, Continuous granulation in the pharmaceutical industry, Chem. Eng. Sci. 60 (14) (2005) 3949–3957. doi:10.1016/j.ces.2005.02.028.

[2] A. El Hagrasy, J. Hennenkamp, M. Burke, J. Cartwright, J. Litster, Twin screw wet granulation: Influence of formulation parameters on granule properties and growth behavior, Powder Technol. 238 (2013) 108–115. doi:10.1016/j.powtec.2012.04.035.

[3] R. M. Dhenge, J. J. Cartwright, M. J. Hounslow, A. D. Salman, Twin screw granulation: Steps in granule growth, Int. J. Pharm. 438 (1-2) (2012) 20–32. doi:10.1016/j.ijpharm.2012.08.049.

[4] J. Vercruysse, D. Córdoba Díaz, E. Peeters, M. Fonteyne, U. Delaet, I. Van Assche, T. De Beer, J. P. Remon, C. Vervaet, Continuous twin screw granulation: Influence of process variables on granule and tablet quality, Eur. J. Pharm. Biopharm. 82 (1) (2012) 205–211. doi:10.1016/j.ejpb.2012.05.010.

[5] M. Fonteyne, S. Soares, J. Vercruysse, E. Peeters, A. Burggraeve, C. Vervaet, J. P. Remon, N. Sandler, T. De Beer, Prediction of quality attributes of continuously produced granules using complementary pat tools, Eur. J. Pharm. Biopharm. 82 (2) (2012) 429–436. doi:10.1016/j.ejpb.2012.07.017.

[6] B. Van Melkebeke, C. Vervaet, J. P. Remon, Validation of a continuous granulation process using a twin-screw extruder, Int. J. Pharm. 356 (1-2) (2008) 224–230. doi:10.1016/j.ijpharm.2008.01.012.

[7] D. Djuric, Continuous granulation with a twin-screw extruder, Cuvillier Verlag, 2008.

[8] M. R. Thompson, J. Sun, Wet granulation in a twin-screw extruder: Implications of screw design, J. Pharm. Sci. 99 (4) (2010) 2090–2103. doi:10.1002/jps.21973.

[9] W.-D. Tu, A. Ingram, J. Seville, Regime map development for continuous twin screw granulation, Chem. Eng. Sci. 87 (2013) 315–326. doi:10.1016/j.ces.2012.08.015.

[10] A. Kumar, K. V. Gernaey, T. De Beer, I. Nopens, Model-based analysis of high shear wet granulation from batch to continuous processes in pharmaceutical production – a critical review, Eur. J. Pharm. Biopharm. 85 (3, Part B) (2013) 814 – 832. doi:10.1016/j.ejpb.2013.09.013.

[11] O. Levenspiel, Chemical Reaction Engineering, 3rd Edition, John Wiley & Sons, 1999.

[12] R. M. Dhenge, R. S. Fyles, J. J. Cartwright, D. G. Doughty, M. J. Hounslow, A. D. Salman, Twin screw wet granulation: Granule properties, Chem. Eng. J. 164 (2-3) (2010) 322–329, Pharmaceutical Granulation and Processing. doi:10.1016/j.cej.2010.05.023.

[13] K. T. Lee, A. Ingram, N. A. Rowson, Twin screw wet granulation: the study of a continuous twin screw granulator using Positron Emission Particle Tracking (PEPT) technique., Eur. J. Pharm. Biopharm. 81 (3) (2012) 666–73. doi:10.1016/j.ejpb.2012.04.011.

[14] S. Bakalis, P. J. Fryer, D. J. Parker, Measuring velocity distributions of viscous fluids using positron emission particle tracking (pept), AIChE J. 50 (7) (2004) 1606–1613. doi:10.1002/aic.10153.

[15] J. Vercruysse, M. Toiviainen, M. Fonteyne, N. Helkimo, J. Ketolainen, M. Juuti, U. Delaet, I. V. Assche,

J. P. Remon, C. Vervaet, T. De Beer, Visualization and understanding of the granulation liquid mixing and distribution during continuous twin screw granulation using NIR chemical imaging, Eur. J. Pharm. Biopharm. 86 (3) (2013) 383–392. doi:10.1016/j.ejpb.2013.10.012.

[16] H. Fogler, Elements Of Chemical Reaction Engineering, Pearson international edition, Prentice Hall Professional Technical Reference, 2006.

[17] A. Gautam, G. S. Choudhury, Screw configuration effects on residence time distribution and mixing in twin-screw extruders during extrusion of rice flour, J. Food Process Eng. 22 (4) (1999) 263–285. doi:10.1111/j.1745-4530.1999.tb00485.x.

[18] R. M. Dhenge, J. J. Cartwright, D. G. Doughty, M. J. Hounslow, A. D. Salman, Twin screw wet granulation: Effect of powder feed rate, Adv. Powder Technol. 22 (2) (2011) 162 – 166. doi:10.1016/j.apt.2010.09.004.